

Dark Soliton Scattering in Symmetric and Asymmetric Double Potential Barriers

F. Tsitoura,¹ Z. A. Anastassi,² J. L. Marzuola,³ P. G. Kevrekidis,^{4,5} and D. J. Frantzeskakis⁶

¹*Dynamics Group, Hamburg University of Technology, 21073 Hamburg, Germany*

²*Department of Mathematics, Statistics and Physics, College of Arts and Sciences, Qatar University, 2713 Doha, Qatar*

³*Department of Mathematics, University of North Carolina, Chapel Hill, NC 27599, USA*

⁴*Department of Mathematics and Statistics, University of Massachusetts, Amherst, Massachusetts 01003-4515 USA*

⁵*Center for Nonlinear Studies and Theoretical Division,*

Los Alamos National Laboratory, Los Alamos, NM 87544

⁶*Department of Physics, National and Kapodistrian University of Athens, Panepistimiopolis, Zografos, Athens 15784, Greece*

Motivated by the recent theoretical study of (bright) soliton diode effects in systems with multiple scatterers, as well as by experimental investigations of soliton-impurity interactions, we consider some prototypical case examples of interactions of dark solitons with a pair of scatterers. In a way fundamentally opposite to the case of bright solitons (but consonant to their “anti-particle character”), we find that dark solitons accelerate as they pass the first barrier and hence cannot be trapped by a second equal-height barrier. A pair of unequal barriers may lead to reflection from the second one, however trapping in the inter-barrier region cannot occur. We also give some examples of dynamical adjusting the barriers to trap the dark soliton in the inter-barrier region, yet we show that this can only occur over finite time horizons, with the dark soliton always escaping eventually, contrary again to what is potentially the case with bright solitons.

I. INTRODUCTION

One of the principal themes within studies of solitons in various physical contexts concerns their interactions with impurities, as well as with potential steps and barriers, within their domain of propagation [1]. In addition to the intrinsic interest of such an area within nonlinear wave theory [2, 3], it is a subject broadly relevant, e.g., to solid state physics [4, 5], and nonlinear optics [6, 7], and it has thus been studied both for bright [8] and dark [9] solitons. In recent years, developments in the physics of atomic Bose-Einstein condensates (BECs) [10–13] have provided a fertile playground where such studies can not only be theoretically extended [14–24], but also experimentally explored. In fact, the combined presence of solitons and defects in BECs has been considered in experimentally relevant setups both for dark [25, 26] (where the motion in the presence of defects has been used to produce the solitons) and bright [27, 28], as well as for dark-bright [29] solitons, in one- and multi-component BECs, respectively.

An intriguing variant of the problem that has been explored recently, is that of inducing soliton trapping and transmission from a pair of defects [30]. A principal finding of the work of Ref. [30], where a bright soliton was scattered from the defects, was the following. As the soliton passed the first defect, it lost some of its energy into radiation, resulting in a reflection from the second one (even if it was of equal size as the first), if the energy was barely over the critical one needed to “overcome” the first defect. This could be used in a two-fold way: considering a weakly asymmetric barrier pair, i.e., a slightly lower on the left and a slightly higher on the right, it was possible to have a bright soliton of the same energy get reflected from the pair of the two barriers when coming from the left, but get transmitted when incident from the right. This principal feature of this configuration was dubbed in the work [30] a “soliton diode” effect. Similar diode features, but for linear wavepackets in lattices with an asymmetric pair of nonlinear elements, were also studied in Refs. [31, 32]. However, an additional remarkable feature of the work of Ref. [30] was the

possibility of trapping of a soliton within a region of two equal barriers. Here, the loss of energy for a weakly “supercritical” barrier interaction results in the soliton energy being “subcritical” with respect to the second barrier and hence unable to overcome it. As a result, the soliton remains forever trapped in the region between the two defects.

Our aim in the present work is to study the scattering dynamics of a dark soliton by two potential barriers, and examine the possibility of soliton trapping, as per the spirit of Ref. [30]. We find that dark solitons behave in a fundamentally different way than bright ones: while bright solitons lose energy and decelerate, being more prone to trapping, dark ones accelerate, thus being amenable to escape dynamics. We find that, while a temporary form of trapping may be enforced by an asymmetric barrier configuration, this is only short lived, because the dark soliton keeps accelerating with each collision, until it eventually overcomes one of the two barriers.

Our presentation of these results will be structured as follows. In section II, we will provide a dynamical systems (theoretical) analysis of the soliton-two barrier interaction. Then, in section III, we will complement this analysis by means of direct numerical simulations. Finally, in section IV, we will provide a summary of our results, as well as number of directions for future study.

II. THEORETICAL ANALYSIS: PARTICLE DYNAMICS

We start our analysis by presenting our model, originating from the context of atomic BECs in the mean-field picture [10]. We consider a quasi one-dimensional (1D) setting whereby a BEC is oriented along the x -direction and is confined in a strongly anisotropic (quasi-1D) trap. In such a setting, the macroscopic wave function $u(x, t)$ satisfies the fol-

lowing dimensionless, 1D Gross-Pitaevskii equation [10–13]:

$$iu_t = -\frac{1}{2}u_{xx} + s|u|^2u + V(x)u, \quad (1)$$

where subscripts denote partial derivatives, $s = +1$ ($s = -1$) corresponds to repulsive (attractive) interatomic interactions, while $V(x)$ is the external potential. In our setting, the latter is assumed to consist of two Gaussian barriers, namely:

$$V(x) = \sum_{i=1}^2 \left\{ V_i \exp \left[-\frac{1}{2} \left(\frac{x - l_i}{\sigma_i} \right)^2 \right] \right\}, \quad (2)$$

where σ_i and V_i set their widths and amplitudes, respectively, while l_i denotes the position of their respective centers. Such a potential may be induced by a pair of far-detuned laser beams, featuring the most natural beam shape, namely the Gaussian profile [11]. Notice that the case $V_i > 0$ ($V_i < 0$) corresponds to blue- (red-) detuned laser beams, that repel (attract) the atoms in the condensate. It is also relevant to mention that in the limit $\sigma_i \rightarrow 0$ the barriers' profile become strongly localized impurities. Furthermore, in the case where $V_i = b_i/(\sqrt{2\pi}\sigma_i)$ (for fixed b_i), the potential (2) features δ -like peaks and can be approximated as:

$$V(x) = \sum_{i=1}^2 b_i \delta(x - l_i). \quad (3)$$

In order to find an effective particle-like equation of motion for the soliton center we follow the analysis of Ref. [14] (see also Ref. [18] for an application in the case of Gaussian barriers). In particular, we first seek stationary solutions of Eq. (1), of the form $u = u_b(x)e^{-i\mu t}$, where the real function $u_b(x)$ represents the spatial profile of the background field, and μ is the chemical potential. Then, it is readily found that $u_b(x)$ satisfies the equation:

$$u_b + \frac{1}{2} \frac{d^2 u_b}{dx^2} - u_b^3 = V(x)u_b, \quad (4)$$

where, without loss of generality, we have fixed the chemical potential at $\mu = 1$.

Let us now assume that the barriers' amplitudes are sufficiently small. In such a case, when the amplitude $\max |u_b(x)|$ is small, the nonlinear term in Eq. (4) can be neglected and, taking into regard that in the homogeneous case ($V(x) = 0$) the background amplitude is equal to 1 when $\mu = 1$, we look for a solution of Eq. (4) in the form:

$$u_b(x) = 1 + f(x), \quad (5)$$

where $f(x)$ incorporates the perturbation by the two Gaussian

barriers and has the approximate form:

$$f(x) = \sqrt{\frac{\pi}{8}} \sum_{i=1}^2 V_i \sigma_i e^{2\sigma_i^2} \times \left\{ \left[-1 + \operatorname{erf} \left(\frac{\sigma_i}{\sqrt{2}} \left(2 + \frac{x - l_i}{\sigma_i^2} \right) \right) \right] e^{2(x-l_i)} + \left[-1 - \operatorname{erf} \left(\frac{\sigma_i}{\sqrt{2}} \left(-2 + \frac{x - l_i}{\sigma_i^2} \right) \right) \right] e^{-2(x-l_i)} \right\}. \quad (6)$$

This way, Eqs. (5)-(6) describe the spatial profile of the effective ground state wavefunction, as modified by the two barriers. Note that in the limiting case of delta-like impurities, the function $f(x)$ can be well approximated by (see Ref. [14] for details):

$$f(x) = -\frac{1}{2} \sum_{i=1}^2 b_i e^{-2|x-l_i|}. \quad (7)$$

To describe the dynamics of a dark soliton on top of this inhomogeneous background, we seek a solution of Eq. (1) in the form

$$u(x, t) = u_b(x) \exp(-it)v(x, t), \quad (8)$$

where the unknown complex field $v(x, t)$ represents a dark soliton. Notice that in the homogeneous case, the dark soliton wavefunction is given by:

$$v(x, t) = \cos \phi \tanh X + i \sin \phi, \quad (9)$$

where $X \equiv \cos \phi [x - x_0(t)]$ is the soliton coordinate, ϕ is the soliton phase angle ($|\phi| < \pi/2$) describing the ‘‘darkness’’ of the soliton, with $\cos \phi$ being the soliton depth ($\phi = 0$ and $\phi \neq 0$ correspond to black and gray solitons, respectively), while $x_0(t)$ and $dx_0/dt = \sin \phi$ denote the position of the soliton center and velocity, respectively.

Substituting Eq. (8) into Eq. (1), a perturbed nonlinear Schrödinger equation for the dark soliton wavefunction is obtained. To treat analytically the soliton motion, we employ the adiabatic perturbation theory developed in Ref. [33] – see Appendix A for more details, as well as the reviews of Refs. [11, 12] for applications of this approach in BECs. This way, the following equation of motion for the soliton center is obtained [18]:

$$\begin{aligned} \frac{d^2 x_0}{dt^2} &= -\frac{dW}{dx_0} \\ &= \sqrt{\frac{\pi}{8}} \sum_{i=1}^2 \left\{ V_i \sigma_i e^{2\sigma_i^2} \int_{-\infty}^{+\infty} [F_{1i}(x) + F_{2i}(x)] dx \right\}, \end{aligned} \quad (10)$$

where the functions $F_{1i}(x)$ and $F_{2i}(x)$ are given by:

$$F_{1i} = \left\{ -1 - \operatorname{erf} \left[\frac{\sigma_i}{\sqrt{2}} \left(-2 + \frac{x - l_i}{\sigma_i^2} \right) \right] \right\} e^{-2(x-l_i)} \\ \times \left[\tanh(x - l_i - x_0) - 1 \right] \\ \times \operatorname{sech}^4(x - l_i - x_0), \quad (11a)$$

$$F_{2i} = \left\{ -1 + \operatorname{erf} \left[\frac{\sigma_i}{\sqrt{2}} \left(2 + \frac{x - l_i}{\sigma_i^2} \right) \right] \right\} e^{2(x-l_i)} \\ \times \left[\tanh(x - l_i - x_0) + 1 \right] \\ \times \operatorname{sech}^4(x - l_i - x_0). \quad (11b)$$

The effective potential $W(x_0)$ can then be determined by numerically integrating Eq. (10). A similar equation of motion for the soliton center can also be found in the limiting case of δ -like impurities, namely:

$$\frac{d^2 x_0}{dt^2} = -\frac{dW}{dx_0} \\ = \frac{3}{8} \sum_{i=1}^2 \left\{ b_i \int_{-\infty}^{+\infty} \operatorname{sgn}(x - l_i) \operatorname{sech}^4(x - x_0) e^{-2|x-l_i|} dx \right\}. \quad (12)$$

In this case too, the effective potential $W(x_0)$ can be found upon integrating Eq. (12). Nevertheless, $W(x_0)$ can be well approximated by a sum of sech^2 functions (cf. Appendix A, as well as Refs. [14, 23] for details) and, thus, $W(x_0)$ reads:

$$W(x_0) \approx \frac{1}{4} \sum_{i=1}^2 b_i \operatorname{sech}^2(x_0 - l_i). \quad (13)$$

An example of the shape of the effective potential $W(x_0)$ for both the Gaussian [dashed (red) line] and δ -like barriers [solid (blue) line] is shown in Fig. 1.

According to the above particle picture for the soliton, a dark soliton incident towards the first barrier can either be reflected or transmitted: if the soliton has a velocity $v = dx_0/dt$ and, thus, a kinetic energy:

$$K = \frac{1}{2} v^2 = \frac{1}{2} \sin^2 \phi \quad (14)$$

smaller (greater) than the maximum W_{\max} of the effective potential, then it will be reflected (transmitted). For low speeds/kinetic energies, one can further use the approximation $\sin \phi \approx \phi$ in identifying the relevant critical point; this consideration leads to $\phi < \phi_c$ or $\phi > \phi_c$ for reflection or transmission, where the critical value ϕ_c of the soliton phase angle is given by (in the small angle approximation):

$$\phi_c \approx \sqrt{2W_{\max}}. \quad (15)$$

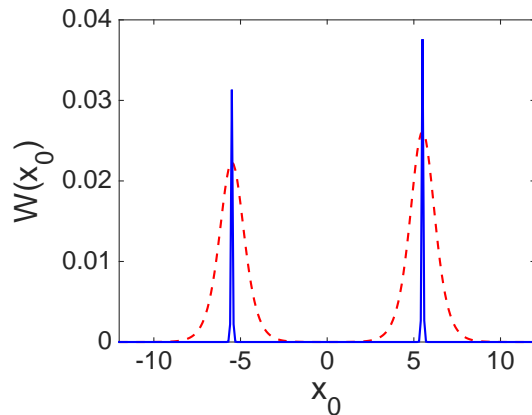


FIG. 1: (Color online) The effective potential $W(x_0)$, in the case of two asymmetric Gaussian barriers [dashed (red) line], for $V_1 = 0.1$, $V_2 = 0.12$, and $\sigma_i = 0.5$ ($i = 1, 2$). Shown also is the limiting case of $\sigma_i \rightarrow 0$, corresponding to the Dirac δ functions [solid (blue) line], for $b_i = V_i \sigma_i \sqrt{2\pi}$, i.e., $b_1 = 0.12$ and $b_2 = 0.15$. In both cases $l_1 = -5.5$ and $l_2 = 5.5$.

III. NUMERICAL RESULTS

A. Bright soliton–two barrier scattering: trapping events

Before we embark on the case of dark solitons in numerical detail, we provide a case example of the trapping scenario that can arise in the case of bright solitons. This is intended to partially motivate our corresponding dark soliton results, and is also partly shown because such a scenario was not explicitly illustrated in Ref. [30]. In particular, we examine Eq. (1) with $s = -1$, in the presence of a Rosen-Morse external potential, namely:

$$V(x) = \sum_{i=1}^2 \left\{ -U_i \operatorname{sech}^2 \left[-\alpha_i (x - l_i) \right] \right\}. \quad (16)$$

Here, U_i , α_i and l_i determine the depth, inverse width, and the position of the center of the first and second potential, respectively. The initial condition which is used has the form of the exact bright soliton solution of the homogeneous version of Eq. (1) for $s = -1$; this solution reads:

$$u(x, t = 0) = A e^{ivx} \operatorname{sech} \left[A (x - x_0) \right], \quad (17)$$

where A sets the amplitude and inverse width of the soliton; this parameter is taken to be $A = 1$. Finally, v and x_0 denote, respectively, the speed and initial position of the soliton.

In Fig. 2, we develop an example, similar to that presented in Ref. [30], using the following parameter values: $U_1 = U_2 = U = 3$, $\alpha_i = 1.73$ for $i = 1, 2$, $l_1 = -6$, $l_2 = 6$. For this set of parameters, and for a bright soliton incident from left to right, the velocity needed for transmission through the first barrier is $v_{cr} = 0.336$ (in fairly good agreement with the semi-analytical prediction $v_{cr} \approx 0.42U^{-0.18} \approx 0.34$ of Ref. [30]). The bright soliton is initially located at $x_0 = -20$

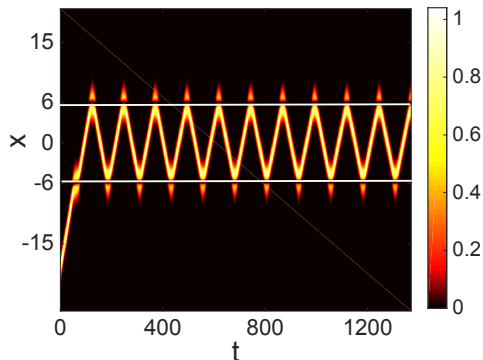


FIG. 2: (Color online) Contour plot for the evolution of a bright soliton density depicting the effect of soliton trapping. The soliton’s initial position and velocity are $x_0 = -20$ and $v = 0.338$, respectively; other parameter values: $U_1 = U_2 = 3$, $\alpha_1 = \alpha_2 = 1.73$, $l_1 = -6$, and $l_2 = 6$.

and has an initial velocity slightly larger than the critical, $v = 0.338$ in the figure. As a result, after it passes the first barrier, the soliton loses part of its energy; hence, its velocity is reduced to $v^* = 0.335$, which is smaller than the critical value for these (identical) barriers. As a consequence, the soliton falls into a (nearly) periodic state –losing a minimal amount of its energy after each collision–, remaining trapped between the two defects. Therefore, in addition to the two velocity regimes of reflection and transmission, there exists also a third narrow parametric regime, whereby the radiation from the first transmission leads to a subcritical incidence speed with respect to the second barrier which, in turn, allows the soliton to become indefinitely trapped.

B. Symmetric potentials

Turning now to the case of dark solitons, our first scenario refers to the case of a symmetric potential, with two Gaussian barriers bearing the same amplitudes (similarly to the bright soliton case studied above). The relevant situation, shown in Fig. 3, corresponds to parameter values $V_1 = V_2 = 0.3$, $\sigma_1 = \sigma_2 = 0.1$, $l_1 = -5.5$ and $l_2 = 5.5$. Here, the energy threshold needed to be overcome by the dark soliton’s kinetic energy in order for the soliton to be transmitted is $W_{\max} = 0.017$; hence, according to Eq. (15), the critical phase angle for transmission/reflection is $\phi_c \approx 0.184$.

We consider a soliton with initial position $x_0 = -10$ and phase angle slightly larger than the critical one, i.e. $\phi = 0.188$ [cf. (red) square point in the phase plane shown in the top panel of Fig. 3]. After the soliton passes the first barrier, it emits radiation in the form of sound waves; as a result (and this is the fundamental difference in the case of the dark solitons, which operate as “negative mass” particles – cf., e.g., Refs. [12]), the soliton becomes shallower and thus faster. In the bottom panel of Fig. 3, where a contour plot depicting the evolution of the soliton density is shown, it is clear that the analytical approximation based on the ordinary differential

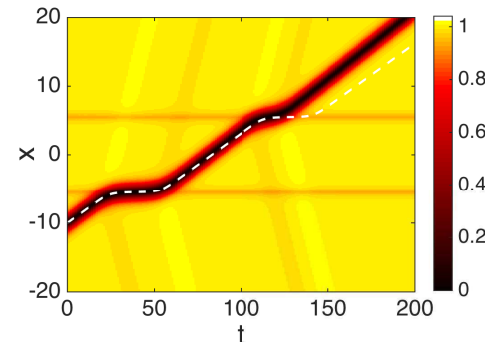
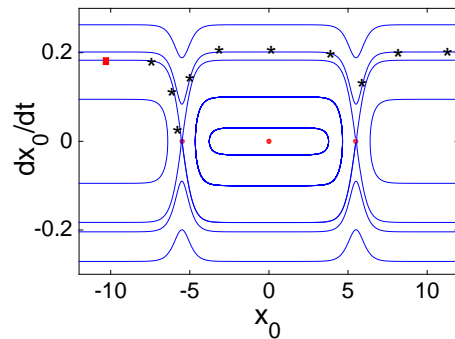


FIG. 3: (Color online) The case of two symmetric Gaussian barriers, with $V_i = 0.3$, $\sigma_i = 0.1$ ($i = 1, 2$), $l_1 = -5.5$ and $l_2 = 5.5$. Top panel: phase plane, where stars depict PDE results showing how the dark soliton accelerates upon incidence. As a result, while starting essentially on the stable manifold of the first saddle point, upon collision with the first barrier accelerates, becoming supercritical with respect to the second saddle point. Bottom panel: contour plot showing the evolution of the dark soliton density for the initial condition depicted in the middle panel with the (red) square, i.e., $x_0 = -10$ and $\phi = 0.188 > \phi_c = 0.183$. The dashed (white) curve depicts the ODE result, which underestimates the distance traveled by the dark soliton (see relevant discussion in the text).

equation (ODE) Eq. (10), underestimates the soliton velocity: the latter, upon incidence to the second barrier, has increased to $\phi \approx 0.2$. As a result, the dark soliton not only avoids trapping (entirely contrary to the case of the bright solitons), but it emerges with a higher kinetic energy (and hence at a larger distance than its theoretically predicted counterpart) after the second barrier. The stars in the phase plane show the corresponding partial differential equation (PDE) results [obtained by direct integration of Eq. (1)]. It is clear from the phase plane evolution that while starting very proximally to the stable manifold of the saddle point at the first barrier, upon incidence, the soliton accelerates (its radiation emission enhances its speed) and, hence, it finds itself definitively over the heteroclinic orbit associated with the second barrier, thus escaping to positive infinity. Qualitatively similar results can also be obtained for a variety of different parameters and are representative of the nature of the dark soliton dynamics.

C. Asymmetric potentials

Motivated by the above observations, the second scenario that we consider concerns the case of slightly asymmetric defects. This allows for regimes where the first defect transmits yet the second one reflects. We thus make the choice of the second barrier being a little higher than the first one. We observe that, as before, the dark soliton becomes shallower after it passes the first barrier and it is accelerated following a different trajectory in the phase plane. Yet, in this case, it may still remain within the region leading to reflection from the second barrier. Nevertheless, when returning to the first, shallower barrier, the dark soliton is supercritical with respect to it, leading to its escape towards minus infinity.

The above configuration is shown in Fig. 4, where we have used $V_1 = 0.3$, $V_2 = 0.34$, $\sigma_1 = \sigma_2 = 0.1$, $l_1 = -5.5$ and $l_2 = 5.5$; in this case, the energy threshold W_{\max} is the same as before, i.e., $W_{\max} = 0.017$. We consider a soliton with initial position $x_0 = -10$ and, as before, a phase angle slightly larger than the critical one, i.e., $\phi = 0.188$ (cf. square (red) point in the phase plane shown in the top panel of Fig. 4). The stars in the phase plane show the corresponding PDE results. Indeed, the soliton velocity after it interacts with the first defect becomes $\phi \approx 0.2$, yet it is still reflected from the asymmetric (taller) second barrier.

Upon return to the first barrier, the soliton exits the trapping region, once again with a larger speed than predicted from the particle picture (dashed line in the figure). Here, too, qualitatively similar results are found for a variety of different parameter values, confirming the acceleration of the dark soliton as a result of its radiation emission.

D. Time-dependent impurities

As we have already shown in the case examples of Figs. 3 and 4, when the soliton interacts with the first defect with a speed close to the critical threshold, it passes the first defect, and then it becomes shallower (and thus faster). If its velocity is still smaller than the critical velocity needed to overcome the second barrier it will there be reflected, but inevitably it will be finally transmitted through the first barrier. Thus, it is not possible to identify a regime for dark soliton trapping, similar to the one found for bright solitons in the case of slightly asymmetric (or symmetric) fixed defects.

Hence, we now focus on the case where the impurities are –and in particular the first one (from the left) is– time-dependent. In such a case, the external potential is of the fol-

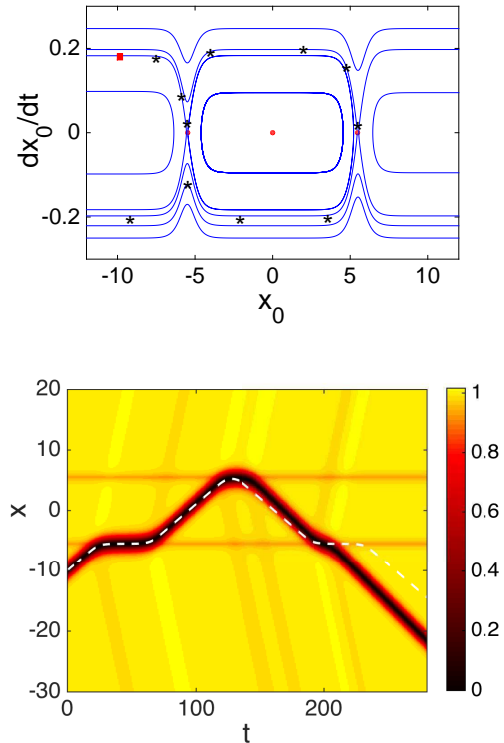


FIG. 4: (Color online) Similar to Fig. 3, but for two asymmetric Gaussian barriers, with $V_1 = 0.3$, $V_2 = 0.34$, $\sigma_1 = \sigma_2 = 0.1$, $l_1 = -5.5$ and $l_2 = 5.5$.

lowing form:

$$\begin{aligned}
 V(x, t) &= V_1(t) \exp \left[-\frac{1}{2} \left(\frac{x - l_1}{\sigma_1} \right)^2 \right] \\
 &\quad + V_2 \exp \left[-\frac{1}{2} \left(\frac{x - l_2}{\sigma_2} \right)^2 \right], \\
 V_1(t) &= \frac{1}{2} \left[(V_1^* + V_1) + (V_1^* - V_1) \tanh \left(\frac{t - t^*}{w^*} \right) \right],
 \end{aligned} \tag{18}$$

where V_1 is the (asymptotic) amplitude of the first barrier before the time t^* , while V_1^* is the (asymptotic) amplitude of the first Gaussian well after that time. Here, we pick t^* as a time after the dark soliton is transmitted through the first barrier but well before it returns to it. In turn, w^* denotes the (chosen to be short) time interval over which the first barrier changes value between its asymptotic limits.

We focus on two different cases. In the first case, the left Gaussian impurity remains repulsive over time, and in the second one it changes sign turning from attractive to repulsive.

For the first case, cf. Fig. 5, we have chosen $V_1 = 0.1$, $V_1^* = 0.5$, $V_2 = 0.5$, $\sigma_1 = \sigma_2 = 0.1$, $l_1 = -5.5$ and $l_2 = 5.5$. We consider a soliton with initial position $x_0 = -10$ and phase angle $\phi = 0.11$, slightly larger than the critical one. After the soliton is transmitted, as expected, from the first barrier it is accelerated but it still has a velocity smaller than the

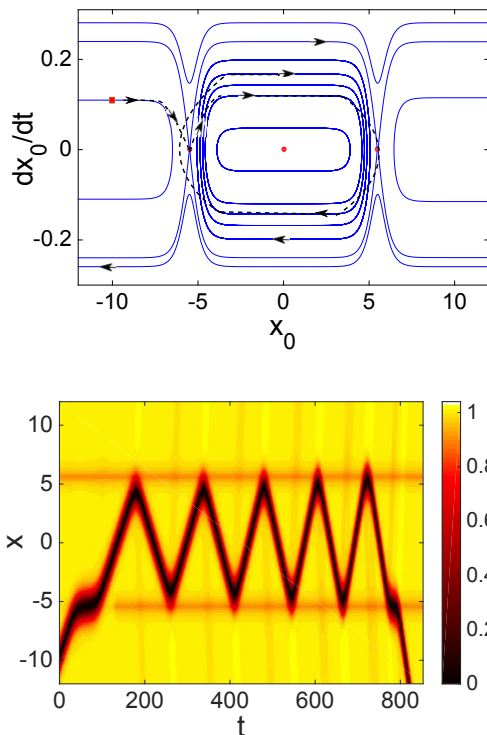


FIG. 5: (Color online) The case where the first Gaussian impurity is time-dependent, and remains repulsive, for $V_1 = 0.1$, $V_1^* = 0.5$, $V_2 = 0.5$, $\sigma_1 = \sigma_2 = 0.1$, $l_1 = -5.5$ and $l_2 = 5.5$. Top panel: corresponding phase plane associated with the final value of the V_1 , i.e. $V_1^* = 0.5$. Dashed (black) line and (black) arrows depict respective PDE results showing the continuous acceleration of the dark soliton that eventually lead to its departure from the trapping region. Bottom panel: contour plot showing the evolution of the dark soliton density for the initial condition depicted in the top panel with the (red) square, i.e., $x_0 = -10$, $\phi = 0.11$.

critical threshold of the second barrier. Meanwhile, the amplitude of the first (left) Gaussian is tuned to become equal to the second (right) Gaussian’s amplitude (notice that, in experimental realizations of such barriers [27, 29], this amounts to a straightforward tuning of the laser beam). Hence, when the dark soliton interacts again with the first barrier it is reflected from it, resulting in an oscillation between the two potential barriers. Nevertheless, as the soliton starts oscillating back and forth now, being temporarily trapped between the two barriers, these oscillations acquire, in fact, progressively smaller period (the soliton keeps getting faster and faster) due to the emitted radiation; as a result, eventually the soliton is transmitted through one of the two barriers.

As observed in Fig. 5, the soliton completes four oscillations before it escapes. We have also tried different parameter values and, as conclusion, for smaller amplitude differences, i.e., $V_1^* - V_1$, we expect less oscillations, while for bigger amplitude differences we observe more oscillations. Nevertheless, in a fashion fundamentally different than its bright soliton counterpart, the “anti-particle” nature of the dark soliton

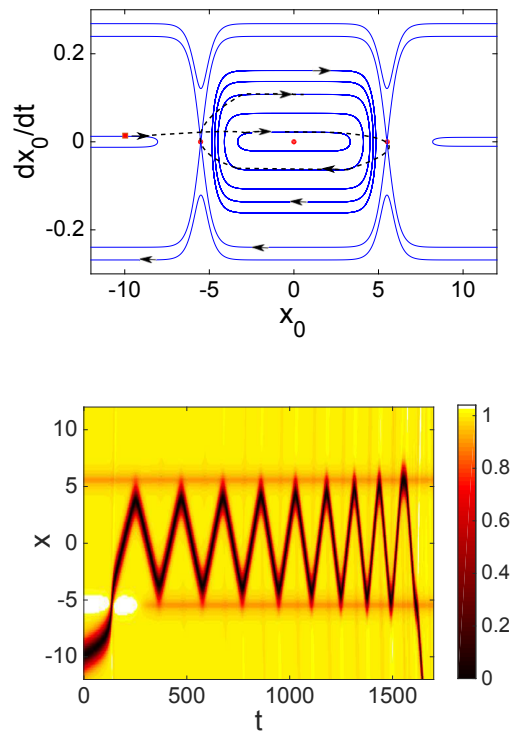


FIG. 6: (Color online) Similar to Fig. 5, but for the case where the first Gaussian impurity is time-dependent, while changing its sign, for $V_1 = -0.5$, $V_1^* = 0.5$, $V_2 = 0.5$, $\sigma_1 = \sigma_2 = 0.1$, $l_1 = -5.5$ and $l_2 = 5.5$. Parameter values for the dark soliton: $x_0 = -10$, $\phi = 0.01$.

and its progressive acceleration will always lead to its expulsion from the trapping region.

This can be also observed in the phase plane associated with the final value of the V_1 , i.e. $V_1^* = 0.5$, shown in the top panel of Fig. 5. The dashed (black) line depicts the first oscillations of the corresponding PDE results. After the soliton interacts with each barrier, it is getting faster following different orbits of an increasing speed—and amplitude—in the phase plane (see (black) arrows). This leads the soliton to follow a spiral trajectory that eventually will allow its departure from the region between the two barriers.

Let us now consider the second case where, initially, the first defect provides a well rather than a barrier, facilitating the dark soliton’s transmission. Relevant results are shown in Fig. 6, where we have used $V_1 = -0.5$, $V_1^* = 0.5$, $V_2 = 0.5$, $\sigma_1 = \sigma_2 = 0.1$, $l_1 = -5.5$ and $l_2 = 5.5$. Again, the phase plane associated with the final value of the V_1 , i.e. $V_1^* = 0.5$, is shown in the top panel of the same figure. The soliton is initially placed at $x_0 = -10$ and it has a phase angle much smaller than before, equals to $\phi = 0.01$.

Here, after the interaction with the first barrier, the soliton’s energy does not change significantly; thus, the soliton is reflected from the second barrier and returns to the first defect which, in the meantime, has become a barrier as well. Given its minimal speed, the dark soliton is able to execute many

oscillations between the two defects in this case, until it is finally able to escape due to the same mechanism as discussed above.

IV. CONCLUSIONS AND FUTURE CHALLENGES

In the present work we have revisited the phenomenon of dark soliton scattering in the presence of a two-defect potential. This was partially motivated by the intriguing findings for bright solitons in the earlier work of Ref. [30]: there, phenomena such as a ‘‘soliton diode’’ were identified in the case of asymmetric barriers, and the possibility of soliton trapping was also predicted even for symmetric potential barriers.

We developed a particle picture allowing us to explore the motion of dark solitons within the realm of two barriers. The most fundamental feature identified was that a scenario of two equal barriers can never trap a dark soliton, fundamentally contrary to what is the case with a bright one. This is because the ‘‘anti-particle’’ character of the dark soliton leads to its increase in speed, upon scattering from the first defect, hence it will always overcome the second defect. Making the barriers asymmetric will not help either, because although the second barrier may reflect the soliton, the first one will always transmit it upon its return, so trapping cannot be achieved. The only possibility for the latter is a phenomenology employing time-dependent barriers. Even here, the dark soliton cannot be trapped indefinitely, yet it can be trapped for long intervals of evolution time, executing many oscillations.

We conjecture that given a very general potential supported sufficiently far from an initial dark soliton, the dark soliton is nonetheless asymptotically stable in that the dynamics lead to a nearby dark soliton moving left or right, depending upon the initial phase angle ϕ . Recent progress on the Gross-Pitaevskii equation with delta function potentials was made in Ref. [2], where orbital stability of stationary dark solitons in the setting of a single δ function potential was proved. The mathematical theory for this setting initiated with the works of Refs. [34, 35].

There are numerous interesting questions for future study that are emerging from the present work. For one thing, it would be especially interesting to explore whether the radiation from the dark soliton could in any analytical (see, e.g., Refs. [36]) or even numerical (see, e.g., Refs. [37]) way be captured. If, especially, analytical results were available then the radiation could be incorporated in the equations of motion, so as to enable a quantitative characterization of the soliton dynamics in the presence of sound waves. Additionally, it would be quite relevant to explore somewhat systematically the phenomenology of scattering in the presence of a double well, rather than a double barrier (see relevant work in Ref. [38]). Finally, extending the relevant considerations to the realm of a larger number of components or a larger dimension would be important. In the former, the examination of the interaction of dark-bright solitons with multiple barriers would be a natural next step [39], while in the latter, exploring the interaction of vortices with such potentials would be of particular interest [11].

Appendix A: Particle dynamics with δ function defects

Here we provide some details on the perturbation theory for dark soliton dynamics in the presence of δ function defects. A similar analysis can also be applied for the case of Gaussian barriers, leading to the results presented in Sec. II.

Our starting point will be the perturbed NLS equation stemming from the substitution of Eq. (8) into Eq. (1):

$$iv_t + \frac{1}{2}v_{xx} - (|v|^2 - 1)v = P(v), \quad (\text{A1})$$

where perturbation $P(v) = 2f(1 - |v|^2)v - (df/dx)v_x$ (with $f(x)$ given in Eq. (7)) can be expressed as follows:

$$P(v) = \sum_{i=1}^2 \left\{ b_i e^{-2u_0|x-l_i|} \left[(1 - |v|^2)v - \text{sgn}(x-l_i)v_x \right] \right\}. \quad (\text{A2})$$

We now employ the adiabatic perturbation theory [11, 12, 33], according to which, the functional form of the soliton remains unchanged, but its parameters x_0 and ϕ become slowly varying functions of time t . In other words, we seek solutions of Eq. (A1) of the form

$$v(x, t) = \cos \phi(t) \tanh X + i \sin \phi(t), \quad (\text{A3})$$

with $X = \cos \phi(t)[x - x_0(t)]$ and

$$x_0(t) = \int_0^t \sin \phi(s) ds. \quad (\text{A4})$$

Then, following energy considerations [11, 12, 33], the following equation for the evolution of the soliton phase angle can be derived:

$$\frac{d\phi}{dt} = \frac{1}{2 \cos^2 \phi \sin \phi} \text{Re} \left(\int_{-\infty}^{\infty} P(v) \bar{v}_t dx \right), \quad (\text{A5})$$

with $P(v)$ and v defined, respectively, in Eqs. (A2) and (A3) above. Notice that only the real part of v is x -dependent, which greatly simplifies calculations. Computing the integral in Eq. (A5), and using the assumption that the solitons are nearly black (i.e., $\phi \rightarrow 0$), we end up with the result:

$$\frac{d\phi}{dt} = \frac{3}{8} \sum_{i=1}^2 \left\{ b_i \int_{-\infty}^{+\infty} \text{sgn}(x-l_i) \text{sech}^4(x-x_0) e^{-2|x-l_i|} dx \right\}. \quad (\text{A6})$$

The integral in the above equation, which is of the form $I = \int_{-\infty}^{+\infty} [\text{sgn}(x) \text{sech}^4(x-x_0) e^{-2|x|}] dx$, can be evaluated using that $I = (2/3) \text{sech}^2(x_0) \tanh(x_0)$. Combining this simplified equation with Eq. (A4), we obtain – from the equation of motion for the soliton center – Eq. (13), namely the effective potential.

Finally, it is worth noticing that a similar feature to the Gaussian barriers occurs in the case of the δ potential barriers as well. In the case of symmetric potentials with $b_1 = b_2 = b$ for instance, it is found that, for a given value of b , there is a critical value of ϕ such that below this critical value the dark

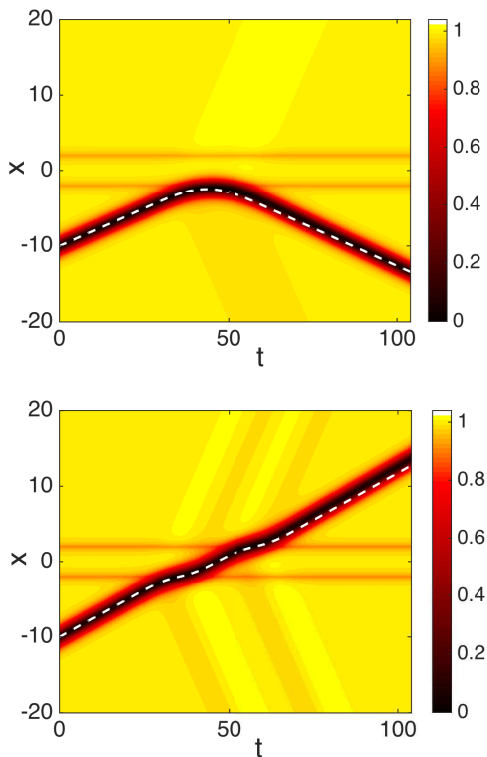


FIG. 7: (Color online) Contour plots showing the evolution of the dark soliton density for two symmetric Dirac delta barriers located at $l_1 = -2$ and $l_2 = 2$; the soliton is initially placed at $x_0 = -10$ and has a phase angle $\phi = 0.2$ (top panel) and $\phi = 0.25$ (bottom panel). The dashed lines show the particle picture from Eq. (12).

soliton is reflected at the first barrier, and above the dark soliton is transmitted through both barriers. A typical example is shown in Fig. 7; note that the full δ potential is simulated using a finite element decomposition, similar to that proposed in Ref. [8], which allows the δ functions to enter in a non-approximate form through the weak formulation of equation (1).

-
- [1] Yu. S. Kivshar and B. A. Malomed, *Rev. Mod. Phys.* **61**, 763 (1989).
- [2] I. Ianni, S. L. Coz, and J. Royer, arXiv:1506.03761.
- [3] J. Holmer, J. Marzuola, and M. Zworski, *Comm. Math. Phys.* **274**, 187 (2007).
- [4] I. M. Lifshitz and A. M. Kosevich, *Rep. Prog. Phys.* **29**, 217 (1966).
- [5] A. M. Kosevich, *Physica D* **41**, 253 (1990).
- [6] A. C. Newell and J. V. Moloney, *Nonlinear Optics* (Addison-Wesley, Redwood City, 1992).
- [7] R. H. Goodman, P. J. Holmes, and M. I. Weinstein, *Physica D* **192**, 215 (2004).
- [8] J. Holmer, J. Marzuola, and M. Zworski, *J. Nonlin. Sci.* **17**, 349 (2007).
- [9] V. V. Konotop, V. M. Pérez-García, Y.-F. Tang, and L. Vázquez, *Phys. Lett. A* **236**, 314 (1997).
- [10] L. P. Pitaevskii and S. Stringari, *Bose-Einstein Condensation* (Oxford University Press, Oxford, 2003).
- [11] P. G. Kevrekidis, D. J. Frantzeskakis, and R. Carretero-González (eds.), *Emergent Nonlinear Phenomena in Bose-Einstein Condensates: Theory and Experiment* (Springer-Verlag, Berlin, 2008); P. G. Kevrekidis, D. J. Frantzeskakis, and R. Carretero-González, *The Defocusing Nonlinear Schrödinger Equation* (SIAM, Philadelphia, 2015).
- [12] R. Carretero-González, D. J. Frantzeskakis, and P. G. Kevrekidis, *Nonlinearity* **21**, 139 (2008); D. J. Frantzeskakis, *J. Phys. A* **43**, 213001 (2010).
- [13] V. S. Bagnato, D. J. Frantzeskakis, P. G. Kevrekidis, B. A. Malomed and D. Mihalache, *Rom. Rep. Phys.* **67**, 5 (2015).
- [14] D. J. Frantzeskakis, G. Theocharis, F. K. Diakonos, P. Schmelcher, and Yu. S. Kivshar, *Phys. Rev. A* **66**, 053608 (2002).
- [15] N. Bilas and N. Pavloff, *Phys. Rev. A* **72**, 033618 (2005).
- [16] N. Bilas and N. Pavloff, *Phys. Rev. Lett.* **95**, 130403 (2005).
- [17] G. Herring, P. G. Kevrekidis, R. Carretero-González, B. A. Malomed, D. J. Frantzeskakis, and A. R. Bishop, *Phys. Lett. A* **345**, 144 (2005).
- [18] I. Hans, J. Stockhofe, and P. Schmelcher, *Phys. Rev. A* **92**, 013627 (2015).
- [19] T. Ernst and J. Brand, *Phys. Rev. A* **81**, 033614 (2010).
- [20] C. Lee and J. Brand, *Europhys. Lett.* **73**, 321 (2006).
- [21] J. L. Helm, T. P. Billam, and S. A. Gardiner, *Phys. Rev. A* **85**, 053621 (2012).
- [22] A. D. Martin and J. Ruostekoski, *New J. Phys.* **14**, 043040 (2012).
- [23] V. Achilleos, P. G. Kevrekidis, V. M. Rothos, and D. J. Frantzeskakis, *Phys. Rev. A* **84**, 053626 (2011).
- [24] F. Tsitoura, Z. A. Anastassi, J. L. Marzuola, P. G. Kevrekidis, and D. J. Frantzeskakis, *Phys. Rev. A* **94**, 063612 (2016).
- [25] P. Engels and C. Atherton, *Phys. Rev. Lett.* **99**, 160405 (2007).

- [26] D. Dries, S. E. Pollack, J. M. Hitchcock, and R. G. Hulet, *Phys. Rev. A* **82**, 033603 (2010).
- [27] A. L. Marchant, T. P. Billam, T. P. Wiles, M. M. H. Yu, S. A. Gardiner, and S. L. Cornish, *Nat. Com.* **4**, 1865 (2013).
- [28] J. Cuevas, P. G. Kevrekidis, B. A. Malomed, P. Dyke, and R. G. Hulet, *New J. Phys.* **15**, 063006 (2013).
- [29] A. Álvarez, J. Cuevas, F. R. Romero, C. Hamner, J. J. Chang, P. Engels, P. G. Kevrekidis, and D. J. Frantzeskakis, *J. Phys. B: At. Mol. Opt. Phys.* **46**, 065302 (2013).
- [30] M. Asad-uz-zaman and U. Al Khawaja, *EPL* **101**, 50008 (2013).
- [31] S. Lepri and G. Casati, *Phys. Rev. Lett.* **106**, 164101 (2011).
- [32] S. Lepri and B. A. Malomed, *Phys. Rev. E* **87**, 042903 (2013); J. D'Ambroise, P. G. Kevrekidis, and S. Lepri, *Chaos* **23**, 023109 (2013); J. D'Ambroise, S. Lepri, B. A. Malomed, and P. G. Kevrekidis, *Phys. Lett. A* **378**, 2824 (2014).
- [33] Yu. S. Kivshar and X. Yang, *Phys. Rev. E* **49**, 1657 (1994).
- [34] P. Gérard, *Ann. Inst. H. Poincaré Anal. Non Linéaire* **23**, 765171 (2006).
- [35] P. Gérard, Vol. **473** of *Contemp. Math.*, pages 12917148. Amer. Math. Soc., Providence, RI (2008).
- [36] D. E. Pelinovsky, Yu. S. Kivshar, and V. V. Afanasjev, *Phys. Rev. E* **54**, 2015 (1996); D. E. Pelinovsky, D. J. Frantzeskakis, and P. G. Kevrekidis, *Phys. Rev. E* **72**, 016615 (2005).
- [37] N. G. Parker, N. P. Proukakis, M. Leadbeater, and C. S. Adams, *Phys. Rev. Lett.* **90**, 220401 (2003); N. G. Parker, N. P. Proukakis, M. Leadbeater, and C. S. Adams, *J. Phys. B* **36**, 2891 (2003); N. G. Parker, N. P. Proukakis, C. F. Barenghi, and C. S. Adams, *ibid.* **37**, S175 (2004); N. P. Proukakis, N. G. Parker, D. J. Frantzeskakis, and C. S. Adams, *J. Opt. B* **6**, S380 (2004).
- [38] A. J. Allen, D. P. Jackson, C. F. Barenghi, and N. P. Proukakis, *Phys. Rev. A* **83**, 013613 (2011).
- [39] P. G. Kevrekidis and D. J. Frantzeskakis, *Reviews in Physics* **1**, 140 (2016).